Collectively, these results demonstrate that (i) lethal synergy of influenza virus and bacterial coinfection can result from loss of tolerance to infection-induced tissue damage, (ii) morbidity and mortality of coinfection can be independent of pathogen burden or excessive inflammatory response, and (iii) promoting tissue repair can, in principle, rescue coinfected animals from morbidity and mortality, even without affecting pathogen burden. Finally, our influenza–*L. pneumophila* coinfection model demonstrates the distinction between resistance and tolerance as separate host defense strategies that can both contribute to morbidity and mortality of infectious disease.

References and Notes

1. L. Råberg, D. Sim, A. F. Read, *Science* **318**, 812 (2007).
2. L. Råberg, A. L. Graham, A. F. Read, *Philos. Trans. R. Soc. London Ser. B Biol. Sci.* **364**, 37 (2009).
3. D. S. Schneider, J. S. Ayres, *Nat. Rev. Immunol.* **8**, 889 (2008).
4. R. Medzhitov, D. S. Schneider, M. P. Soares, *Science* **335**, 936 (2012).
5. C. Beadling, M. K. Slifka, *Curr. Opin. Infect. Dis.* **17**, 185 (2004).
6. J. A. McCullers, *Clin. Microbiol. Rev.* **19**, 571 (2006).
7. J. M. Hament, J. L. Kimpen, A. Fleer, T. F. Wolfs, *FEMS Immunol. Med. Microbiol.* **26**, 189 (1999).
8. V. T. Peltola, J. A. McCullers, *Pediatr. Infect. Dis. J.* **23** (suppl.), S87 (2004).
9. M. Iannuzzi *et al.*, *J. Med. Case Rep.* **5**, 520 (2011).
10. A. Shahangian *et al.*, *J. Clin. Invest.* **119**, 1910 (2009).
11. A. R. Iverson *et al.*, *J. Infect. Dis.* **203**, 880 (2011).
12. K. Sun, D. W. Metzger, *Nat. Med.* **14**, 558 (2008).
13. A. Didierlaurent *et al.*, *J. Exp. Med.* **205**, 323 (2008).
14. K. H. Berger, R. R. Isberg, *Mol. Microbiol.* **7**, 7 (1993).
15. D. B. Mendel *et al.*, *Antimicrob. Agents Chemother.* **42**, 640 (1998).
16. T. Ichinohe, *Expert Rev. Vaccines* **9**, 1315 (2010).
17. A. García-Sastre, C. A. Biron, *Science* **312**, 879 (2006).
18. T. Ren, D. S. Zamboni, C. R. Roy, W. F. Dietrich, R. E. Vance, *PLoS Pathog.* **2**, e18 (2006).
19. A. B. Molofsky *et al.*, *J. Exp. Med.* **203**, 1093 (2006).
20. D. S. Zamboni *et al.*, *Nat. Immunol.* **7**, 318 (2006).
21. K. A. Archer, C. R. Roy, *Infect. Immun.* **74**, 3325 (2006).
22. R. Spörri, N. Joller, U. Albers, H. Hilbi, A. Oxenius, *J. Immunol.* **176**, 6162 (2006).
23. N. L. La Gruta, K. Kedzierska, J. Stambas, P. C. Doherty, *Immunol. Cell Biol.* **85**, 85 (2007).
24. J. S. M. Peiris, K. P. Y. Hui, H.-L. Yen, *Curr. Opin. Immunol.* **22**, 475 (2010).
25. N. Schmitz, M. Kurrer, M. F. Bachmann, M. Kopf, *J. Virol.* **79**, 6441 (2005).
26. T. Decker, M. Müller, S. Stockinger, *Nat. Rev. Immunol.* **5**, 675 (2005).
27. M. F. Fontana, S. Shin, R. E. Vance, *Infect. Immun.* **80**, 3570 (2012).
28. D. K. Bhalla, *J. Toxicol. Environ. Health B Crit. Rev.* **2**, 31 (1999).
29. L. M. Crosby, C. M. Waters, *Am. J. Physiol. Lung Cell. Mol. Physiol.* **298**, L715 (2010).
30. H. R. Wong, J. R. Wispé, *Am. J. Physiol.* **273**, L1 (1997).
31. L. A. Monticelli *et al.*, *Nat. Immunol.* **12**, 1045 (2011).

Acknowledgments: We thank S. Holley and C. Annicelli for technical assistance; T. Ichinohe, M. Linehan, and A. Iwasaki for viral strains and advice; T. Ren, M. Fontana, R. Vance, K. Archer, S. Shin, and C. Roy for *L. pneumophila* strains and advice; M. Gillum for assistance with experiments; and M. Mueller and C. Lassnig for mouse infection infrastructure. The data presented in the manuscript are tabulated in the main paper and in the supplementary materials. This work was supported by the Howard Hughes Medical Institute (R.M.), NIH grants R01 046688 and AI R01 055502 (R.M.), the Ellison Foundation (R.M.), the New England Regional Center of Excellence (R.M.), and FWF (Austrian Science Fund) grant P25235-B13 (A.M.J.). A.M.J. was a Berger Foundation fellow of the Damon Runyon Cancer Research Foundation. The authors have no conflicts of interest.

Supplementary Materials

www.sciencemag.org/cgi/content/full/science.1233632/DC1
Supplementary Text
Figs. S1 to S6
References (*32*, *33*)

4 December 2012; accepted 15 April 2013
Published online 25 April 2013;
10.1126/science.1233632

Repeated Cortico-Striatal Stimulation Generates Persistent OCD-Like Behavior

Susanne E. Ahmari,[1,2,3,4]* Timothy Spellman,[5] Neria L. Douglass,[1,2] Mazen A. Kheirbek,[1,2] H. Blair Simpson,[1,3,4] Karl Deisseroth,[6] Joshua A. Gordon,[1,2] René Hen[1,2]

Although cortico-striato-thalamo-cortical (CSTC) circuit dysregulation is correlated with obsessive compulsive disorder (OCD), causation cannot be tested in humans. We used optogenetics in mice to simulate CSTC hyperactivation observed in OCD patients. Whereas acute orbitofrontal cortex (OFC)–ventromedial striatum (VMS) stimulation did not produce repetitive behaviors, repeated hyperactivation over multiple days generated a progressive increase in grooming, a mouse behavior related to OCD. Increased grooming persisted for 2 weeks after stimulation cessation. The grooming increase was temporally coupled with a progressive increase in light-evoked firing of postsynaptic VMS cells. Both increased grooming and evoked firing were reversed by chronic fluoxetine, a first-line OCD treatment. Brief but repeated episodes of abnormal circuit activity may thus set the stage for the development of persistent psychopathology.

OCD is characterized by intrusive distressing thoughts (obsessions) and/or repetitive mental or behavioral acts (compulsions) and is a leading cause of illness-related disability (*1*, *2*). Although the pathophysiology underlying OCD is unclear, multiple lines of evidence implicate dysregulation within cortico-striato-thalamo-cortical (CSTC) circuits (*3*–*6*). Specifically, functional imaging studies suggest that hyperactivity in orbitofrontal cortex (OFC) and ventromedial striatum (VMS) is associated with OCD pathology (*5*, *7*, *8*). Furthermore, successful treatments are associated with reductions in hyperactivity (*9*, *10*). However, it is not known if OFC-VMS hyperactivity can directly cause OCD symptoms, because increased activity could represent adaptive, homeostatic, or unrelated processes compensating for other primary abnormalities. We therefore used an optogenetic strategy to directly test whether hyperstimulation of glutamatergic OFC-VMS projections leads to OCD-like behaviors in mice.

A Cre-inducible adenovirus-associated vector (AAV) carrying the gene encoding channelrhodopsin (ChR2) fused to enhanced yellow fluorescent protein (EYFP) [pAAV-Ef1a-DIO-ChR2 (H134R)-EYFP; referred to as DIO-ChR2] (*11*) was stereotactically injected into OFC of EMX-Cre transgenic mice to ensure specific ChR2 expression in cortical glutamatergic neurons (Fig. 1A) (*12*). Cortical Cre expression led to sustained expression of ChR2-EYFP (Fig. 1B). Unilateral 473-nm stimulation through chronic fiber-optic implants in OFC yielded lateralized increased activation of the immediate early gene c-*fos* ($P < 0.009$) (Fig. 1, C and D), which demonstrated in vivo cellular activation by laser stimulation. Two weeks postinjection, EYFP staining was seen in OFC cell bodies and axons projecting to VMS (Fig. 1E), which indicated targeting of OFC-VMS projections. In vitro recordings in cortico-striatal slices demonstrated VMS field responses after 473-nm laser stimulation of OFC axon terminals in striatum (Fig. 1F). To verify adequate stimulation of ChR2-expressing OFC-VMS terminals in vivo, we implanted stereo opto-electrodes (optrodes) into VMS that permit combined fiber-optic stimulation and 32-channel simultaneous recording of multiple single units (Fig. 1G). In awake behaving mice, in vivo recordings demonstrated robust VMS field responses after 473-nm laser stimulation of OFC axon terminals in striatum (Fig. 1, H and I), which showed

[1]Department of Psychiatry, Columbia University College of Physicians and Surgeons, New York, NY 10032, USA. [2]Division of Integrative Neuroscience, New York State Psychiatric Institute, New York, NY 10032, USA. [3]Division of Clinical Therapeutics, New York State Psychiatric Institute, New York, NY 10032, USA. [4]Anxiety Disorders Clinic and OCD Research Program, New York State Psychiatric Institute, New York, NY 10032, USA. [5]Department of Physiology, Columbia University College of Physicians and Surgeons, New York, NY 10032, USA. [6]Departments of Psychiatry and Bioengineering, Stanford University School of Medicine, Stanford, CA 94305, USA.
*Corresponding author. E-mail: sea2103@columbia.edu

feasibility of activation of specific cortical-VMS projections.

Because patients with OCD have hyperactivity in OFC-striatal circuits (*3*–*6*), we predicted that direct elevation of OFC-VMS activity would lead to increases in OCD-related behaviors including grooming, anxiety, and prepulse inhibition (PPI) deficits (*13*). We injected DIO-ChR2 into the left OFC of EMX-Cre mice and implanted fiber-optic probes unilaterally in left VMS (Fig. 2A). After waiting 3 to 4 weeks for surgical recovery and stable viral expression, we habituated mice to the open field and fiber-optic stimulation apparatus. We then repeatedly elevated activity in OFC-VMS projections by stimulating for 5 min at 10 Hz for five consecutive days (10 ms, 1 to 5 mW) (*14*). Grooming behavior was recorded with digital video and scored by blind raters for 5 min before (Pre), during (Stim), and after (Post) stimulation (Fig. 2B). Whereas acute OFC-VMS stimulation did not produce grooming, a small but significant progressive increase in grooming time was noted during the prestimulation period on consecutive days (Fig. 2C) [repeated measures analysis of variance (ANOVA), main effect: $P < 0.048$; $F = 4.43$; Fisher's protected least significant difference (PLSD): for day 3, $P < 0.03$; for day 5, $P < 0.047$]. Because the prestimulation measurement on days 2 to 5 served as a 24-hour time stamp for effects of stimulation the day before, this suggested that repeated stimulation led to chronic circuit changes that ultimately resulted in sustained, stimulation-independent OCD-like behavior. Although it is possible that stress from handling contributed to the grooming increase in the prestimulation period, stress was minimized by habituation to fiber-optic tethering daily for a week before data collection and was identical for controls and ChR2+ mice. To resolve the time-course of the grooming increase, we examined a new cohort an hour after stimulation ($Groom_{1\ hour\ post}$) (Fig. 2D). We observed a dramatic progressive increase in grooming over consecutive days using this measure (main effect: $P < 0.02$; $F = 7.32$) (Fig. 2E). Although total grooming time increased, there was not a significant increase in stereotyped syntactic grooming chains in ChR2+ animals on day 5 of stimulation (table S1). No differences in grooming time were observed between controls and ChR2+ animals on day 1 of stimulation, which indicated that ChR2 expression without laser stimulation did not lead to an increase in grooming. Notably, increased grooming persisted even

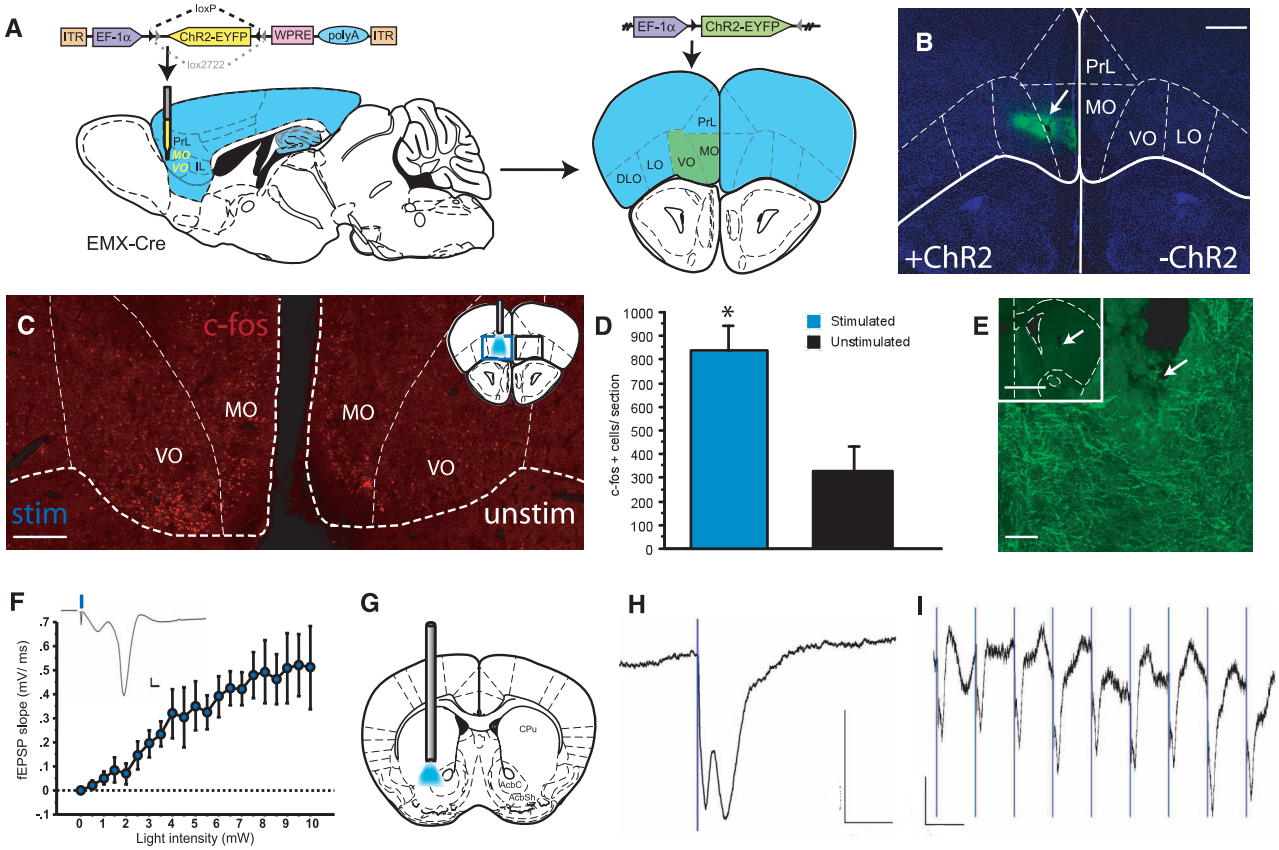

Fig. 1. Injection of ChR2-EYFP AAV into OFC leads to functional ChR2 expression in projections from OFC to VMS. (**A**) Schematic diagram of DIO-ChR2 injections. (Left) Reference sagittal section indicates injection position in ventromedial OFC (VO/MO) of EMX-Cre mice (2.6 mm AP, 1.7 mm DV, 0.5 mm ML). Blue shading: Cre expression in cortex and hippocampus. (Right) Cre-expressing glutamatergic cells in OFC irreversibly invert the ChR2-EYFP open reading frame, which leads to cell type–specific ChR2-EYFP expression (green shading). EF-1α, elongation factor 1α; ITR, inverted terminal repeat; WPRE, woodchuck hepatitis virus posttranslational regulatory element; DLO, dorsolateral orbitofrontal cortex; LO, lateral orbitofrontal cortex; PrL, prelimbic cortex. (**B**) Confocal image of YFP-immunostaining shows unilateral ChR2 expression at OFC injection site. Scale bar, 500 μm. (**C**) c-Fos immunostaining demonstrates 473-nm light–induced activation of OFC in awake behaving mice through chronic fiber-optic implant. (Inset) Reference coronal section. Blue square, stimulated; black, unstimulated. (**D**) Quantification of c-Fos–positive cells in stimulated versus unstimulated OFC ($P < 0.009$) ($n = 4$ controls; 4 ChR2 mice; five sections each). (**E**) Targeting of OFC-VMS projections evidenced by axonal YFP staining under fiber-optic implant site (arrow). Scale bar, 100 μm. (Inset) Low magnification. Scale bar, 500 μm. (**F**) Extracellular field recordings from striatal slices. Increased population spike amplitude with increasing laser power. (Inset) Individual population spike after 0.1-ms light pulse (3 mW); calibration bars: vertical 0.5 mV, horizontal 1 ms. $n = 4$ slices from each of three animals. (**G**) Schematic diagram of stereo-optrode implant in VMS. (Stereotaxic coordinates: 0.98 mm AP, 3.5 mm DV, 1.25 mm ML). CPu, caudate putamen; AcbC, accumbens core; AcbSh, accumbens shell. (**H**) In vivo recordings in awake behaving animals show field responses to 473-nm stimulation of VMS terminals. Mean response to 20 flashes delivered at 0.5 Hz. Calibration bar: vertical 0.5 mV, horizontal 20 ms. (**I**) Raw responses to train of 10 flashes at 10 Hz. Calibration bar: vertical 0.5 mV, horizontal 100 ms.

in the absence of stimulation up to 2 weeks later ($P < 0.03$) (Fig. 2F).

Acute OFC-VMS stimulation led immediately to a large but transient increase in locomotion compared with controls; no differences were observed pre- or poststimulation (fig. S1A). To ensure that increased grooming was not simply a consequence of increased locomotion, we injected DIO-ChR2 and implanted fiber optics in motor cortex (M2) of EMX-Cre mice (fig. S1B). The 5-day stimulation paradigm described above led to increased locomotion (fig. S1C) but not to increased grooming (fig. S1D), which suggested that increased grooming was not simply a side effect of overall increased activity. To determine the specificity of OFC-VMS pathway hyperactivation in induction of persistent grooming, we injected AAV-ChR2 into infralimbic and prelimbic cortex (IL/PrL) (fig. S2A) and stimulated IL/PrL–VMS projections using our 5-day stimulation paradigm. Repeated stimulation of IL/PrL–VMS projections did not lead to a progressive increase in grooming behavior (fig. S2, B to D).

Other OCD-associated behavioral measures were tested after completion of the 5-day stimulation paradigm. No differences were seen in PPI (*13*) or anxiety levels (in open field and elevated plus maze) compared with testing before stimulation (fig. S3); in addition, no changes in open field anxiety were observed during acute stimulation (fig. S4). Together, these results suggest that repeated stimulation of OFC-VMS projections led to specific induction of repetitive behavior.

We next examined electrophysiologic changes correlated with the progressive grooming increase using VMS stereo-optrodes (Fig. 3A and fig. S5). In awake behaving mice, recordings of multiple single units in the VMS were obtained during the 15-min stimulation protocol and 1 hour post grooming assessment (Fig. 3B). Light-evoked responses were observed in individual units in response to 10 Hz stimuli (Stim) or 0.1 Hz probe pulses (used to measure light-evoked activity during pre-, post-, and 1 hour poststimulation) over 5 days of repeated stimulation. Cells displayed a range of responses to light pulses, including activation (Fig. 3C), suppression (Fig. 3D), and no effect (Fig. 3E); we therefore used each cell's stimulation-induced change in firing rate (expressed as a *Z*-score; see supplementary methods) to assess responsiveness to afferent stimulation. Across 5 days of stimulation, mean responses increased both during stimulation and 1 hour poststimulation (Fig. 3F; $R = 0.21$ and 0.28; $P < 0.002$ and < 0.001, respectively). *Z*-scores were greater on day 5 than on day 1, which indicated increased evoked firing (at 10 Hz: $P < 0.02$; at 0.1 Hz: $P < 0.004$). Thus, repeated hyperstimulation led to a marked progressive increase in light-evoked firing paralleling the increase in repetitive behavior.

Finally, we determined whether a medication regimen used to treat OCD would reverse the increases in repetitive behavior and evoked VMS activity. After 7-day grooming induction, we initiated fluoxetine treatment (18 mg/kg body weight per day) while continuing daily stimulation (Fig. 4A). Fluoxetine was chosen because serotonin reuptake inhibitors (SRIs) are the only proven monotherapy for OCD (*15*). Although there was no effect of fluoxetine after 1 week, 2 weeks of treatment led to a reversal of grooming behavior to control levels (Fig. 4B) (main effect: $P < 0.009$, $F = 9.53$; Fisher's PLSD: baseline versus week 2,

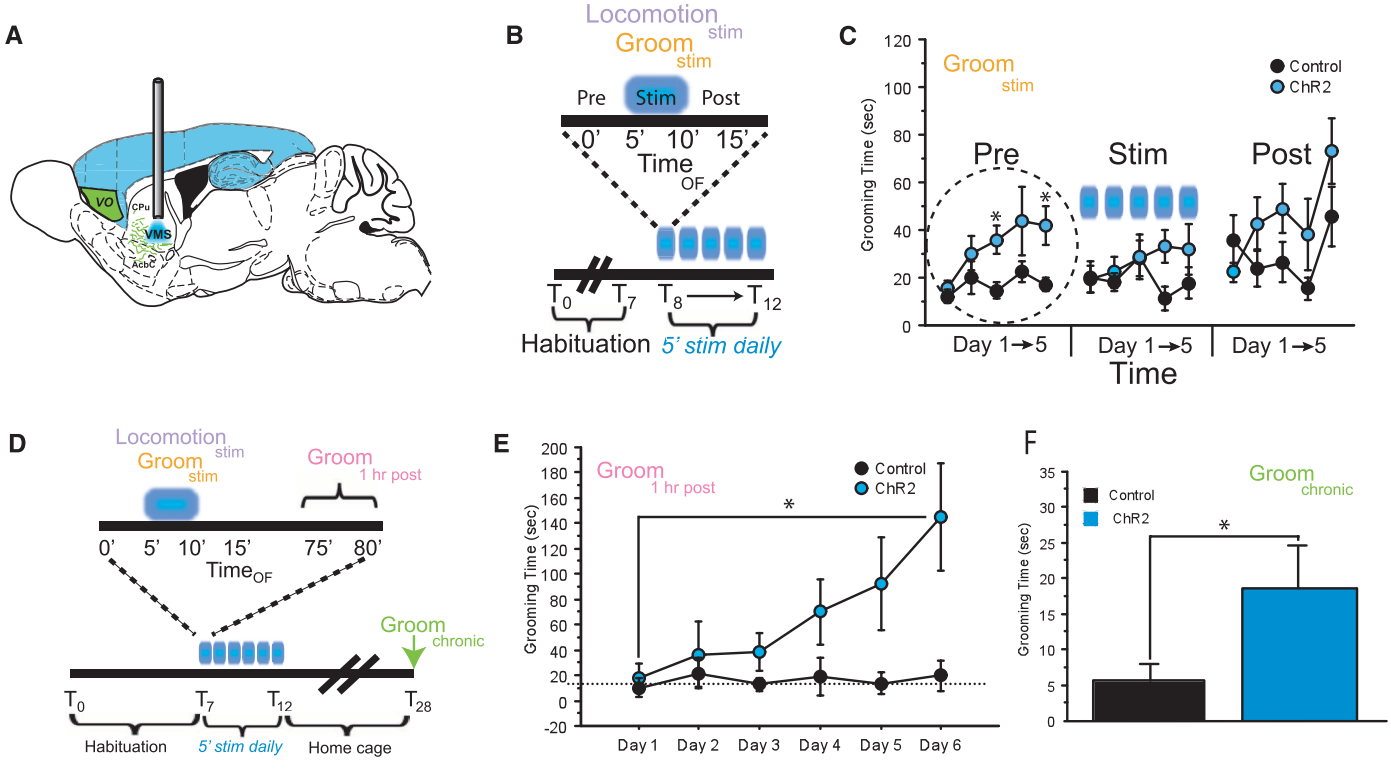

Fig. 2. Brief repeated hyperstimulation of OFC-VMS projections leads to progressively increased grooming behavior. (**A**) Localization of viral injection and fiber-optic implant. ChR2 (green) is expressed in ventromedial OFC. Fiber-optic implant is placed into VMS to stimulate ChR2 in axon terminals projecting from OFC. (**B**) Time line for chronic stimulation of OFC-VMS projections. After habituation to the tethering procedure for 7 days (T_1 to T_7), mice underwent the stimulation protocol. $Time_{OF}$ = Time in open field. (**C**) Grooming behavior over five consecutive days of stimulation. Total time grooming was assessed for 5 min before (Pre), during (Stim), and after stimulation (Post) for five consecutive days. Data are grouped into Pre, Stim, and Post categories for days 1 to 5 to facilitate examination of changes in behavior over time. Stimulation (10 Hz) led to a significant increase in grooming time in ChR2 animals before stimulation (Pre) (main effect: $P < 0.048$, $F = 4.43$; post hoc test: day 3, $^*P < 0.03$; day 5, $^*P < 0.047$; $n = 8$ ChR2 mice, 7 controls). (**D**) Time line for examination of chronic impact of stimulation. (**E**) After 6 days of stimulation, ChR2+ animals had significantly elevated grooming during $Groom_{1\ hour\ post}$ (main effect $^*P < 0.02$; $F = 7.32$; *n* count: ChR2 = 6; control = 5). (**F**) Two weeks after repeated stimulation (T_{28}), ChR2+ animals continued to demonstrate significantly increased grooming ($Groom_{chronic}$ $^*P < 0.03$; one-tailed *t* test), although absolute grooming time was decreased compared with times immediately after stimulation paradigm (T_{12}).

$P < 0.003$). This delayed response is consistent with the delayed onset of effective SRI treatment in OCD patients. We also repeated this experiment using a vehicle control group (Fig. 4C). Again, 2 weeks of fluoxetine led to reversal of induced grooming (Fig. 4D). Moreover, in a separate cohort of stereo-optrode–implanted animals, the increase in light-evoked activity induced by repeated 10 Hz stimulation was normalized after chronic fluoxetine (Fig. 4, E and F).

Repeated hyperactivation of OFC-VMS projections generates a progressive increase in grooming, temporally linked to a cumulative increase in VMS light-evoked firing. Acute stimulation of the OFC-VMS pathway was not sufficient to produce OCD-relevant excessive grooming (*3*, *16*–*18*). The behavioral change was persistent, becoming stimulation-independent within 6 days. Although classic theories suggest that abnormal repetitive behaviors, including OCD symptoms, directly result from hyperactivity in CSTC loops (*19*–*21*), causation has been difficult to prove. Though genetic and pharmacologic manipulations of norepinephrine and dopamine can lead to transient increases in repetitive behaviors (*22*), the interventions were not limited to specific circuits, and associated electrophysiologic changes were observed in multiple brain regions. Our optogenetic system permits activation of specific cortico-striatal circuits and genetic definition of the activated cell-type as cortical glutamatergic projection neurons.

Our in vivo electrophysiology data suggest a circuit-based mechanism for establishment of repetitive behaviors. Repeated hyperstimulation led to a marked progressive increase in light-evoked firing paralleling the increase in grooming, suggesting plasticity at OFC-VMS synapses that builds over consecutive days. We speculate that brief episodes of light-induced activity lead to long-lasting changes that prime OFC-VMS synapses, decreasing the activation threshold during subsequent bouts of stimulation. In turn, increased activity at OFC-VMS synapses may transmit information through the CSTC circuit (*23*–*25*) and lead to multiple downstream events that ultimately reinforce repetitive behaviors, including (i) plasticity in downstream structures such as thalamus and prefrontal cortex (*26*), and (ii) increased motivational saliency mediated by the ventral tegmental area (*22*). This mechanism would be consistent with the observed fluoxetine effects, since selective SRIs have been shown to reduce primary reward processing (*27*, *28*).

OCD is a heterogeneous disorder. Our study therefore may have greater relevance for particular OCD subtypes. For example, dimensional models of OCD have been proposed in which different types of obsessions and compulsions are associated with different circuits (*29*, *30*). Because our results suggest that repeated stimulation of OFC-VMS projections led to specific induction of repetitive grooming, our model may be of particular importance for OCD patients with predominant contamination concerns.

Our findings yield new insight into how psychopathology could develop. Only 5 min of stimulation per day was sufficient to lead to sustained significant behavioral effects. This raises the possibility that pathological changes, including compulsions in OCD, may result from small but repeated bursts of abnormal neuronal activity and also offers suggestions for new treatment approaches or refinements of existing therapies for disorders characterized by repetitive behaviors. For example, our data are consistent with recent clinical studies demonstrating efficacy of ventral capsule–ventral striatum deep brain stimulation in OCD (*31*, *32*), which is thought to act via inhibition of OFC hyperactivity. Optogenetic approaches could be used to dissect circuit mechanisms underlying deep brain stimulation and other treatments, with a goal of identifying new treatment targets.

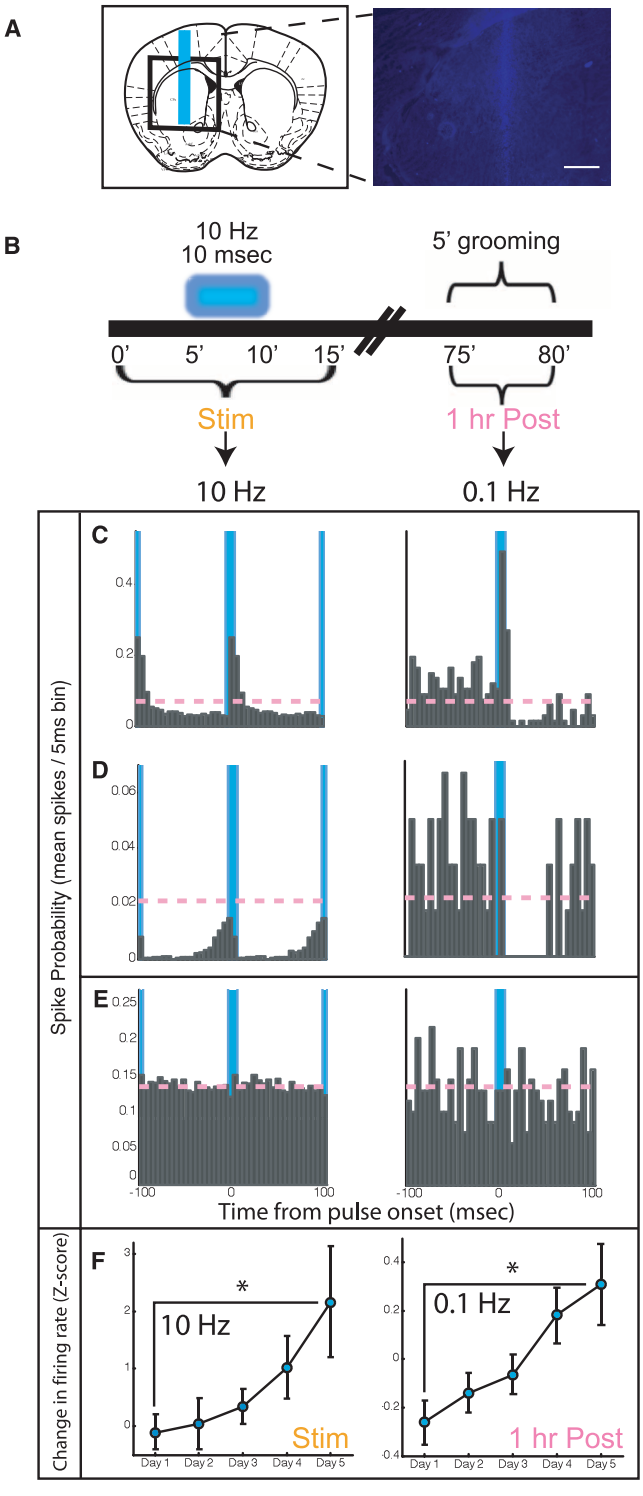

Fig. 3. Repeated daily stimulation of OFC-VMS projections leads to increased evoked firing. (**A**) (Left) Schematic diagram of stereo-optrode implant site. (Right) Placement visualized via implanting a stereo-optrode dipped in Hoecsht stain (1:1000). Scale bar, 500 μm. (**B**) Stimulation protocol used for in vivo recording. (**C** to **E**) Representative peristimulus spike histograms (5-ms time bins) of three neurons recorded during 10 Hz stimulation (left) and 0.1 Hz probe pulses (1 hour poststimulation on right). Baseline spontaneous firing rate for each cell is shown as pink dashed line. Cells exhibited varied stimulus responsiveness, including evoked activation (C), evoked suppression (D), and no response (E). (**F**) Light-evoked firing (measured by peristimulus *z*-scores) across 5 days of stimulation both during 10 Hz stimulation (Stim) and during 0.1 Hz probe pulses 1 hour after stimulation (1 hour post) (*$P < 0.021$ and $P < 0.004$). Negative *Z*-scores for 0.1 Hz on days 1 and 2 indicate net suppression of evoked firing rate during $\text{Groom}_{1\ \text{hour post}}$ after the first two epochs of 10 Hz stimulation.

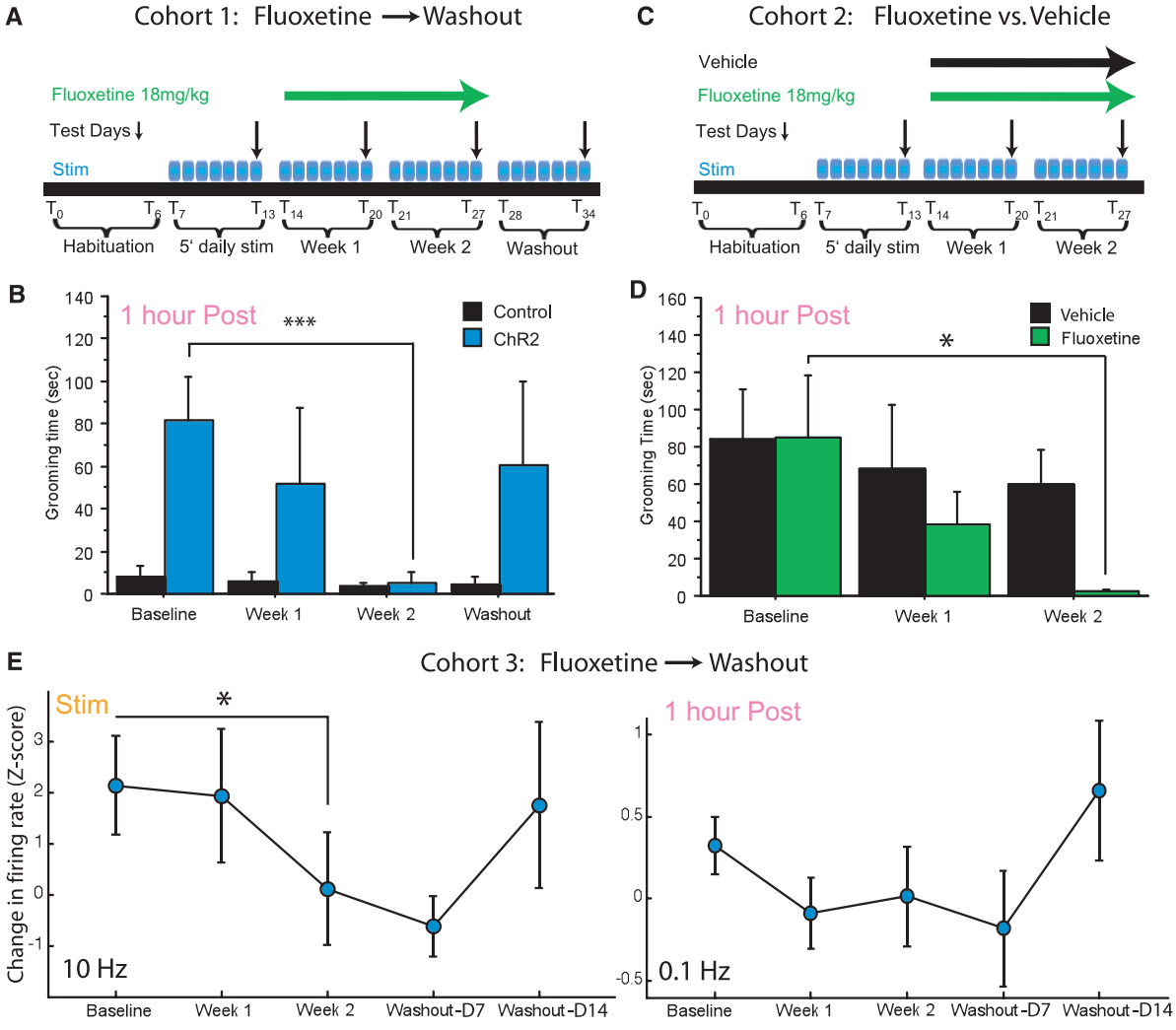

Fig. 4. Perseverative grooming and elevated evoked firing rate are resolved by chronic, but not acute, fluoxetine treatment. (**A**) Experimental time line for fluoxetine wash-out experiment. (**B**) Two weeks of fluoxetine treatment reduced grooming to level of controls. Main effect: $P < 0.009$; $F = 9.53$; Fisher's PLSD: baseline versus week 2, $^{***}P < 0.003$. Increased grooming was reestablished after a 1-week fluoxetine wash-out. Main effect: $P < 0.09$; $F = 3.58$. n values: ChR2^{+} mice = 8; controls = 7. (**C**) Experimental time line for fluoxetine versus vehicle experiment. (**D**) Two weeks of fluoxetine treatment reduced grooming to levels of vehicle-treated animals. Main effect: $P < 0.14$; $F = 2.59$; Fisher's PLSD: baseline versus week 2, $^{*}P < 0.04$. Fluoxetine: $n = 7$; vehicle: $n = 6$. (**E**) (Left) In stereotrode–implanted animals, peristimulus Z-scores for 10 Hz stimuli normalized after 2 weeks of fluoxetine ($P < 0.028$); after 2-week wash-out, Z-scores returned to pretreatment levels. (Right) Peristimulus Z-scores for 0.1 Hz probe pulses showed a nonsignificant decrease after fluoxetine treatment, which returned to pretreatment levels after wash-out.

References and Notes

1. C. J. L. Murray, A. D. Lopez, *The Global Burden of Disease: A Comprehensive Assessment of Mortality and Disability from Diseases, Injuries, and Risk Factors in 1990 and Projected to 2020*, Global burden of disease and injury series; vol. 1 (Harvard School of Public Health, Harvard Univ. Press, Cambridge, MA, 1996).
2. R. C. Kessler *et al.*, *Arch. Gen. Psychiatry* **62**, 593 (2005).
3. J. T. Ting, G. Feng, *Curr. Opin. Neurobiol.* **21**, 842 (2011).
4. R. Marsh, T. V. Maia, B. S. Peterson, *Am. J. Psychiatry* **166**, 664 (2009).
5. M. R. Milad, S. L. Rauch, *Trends Cogn. Sci.* **16**, 43 (2012).
6. C. Pittenger, M. H. Bloch, K. Williams, *Pharmacol. Ther.* **132**, 314 (2011).
7. S. Saxena, R. G. Bota, A. L. Brody, *Semin. Clin. Neuropsychiatry* **6**, 82 (2001).
8. J. Y. Rotge *et al.*, *Biol. Psychiatry* **65**, 75 (2009).
9. S. L. Rauch, C. R. Savage, N. M. Alpert, A. J. Fischman, M. A. Jenike, *Biol. Psychiatry* **42**, 446 (1997).
10. J. L. Abelson *et al.*, *Biol. Psychiatry* **57**, 510 (2005).
11. H. C. Tsai *et al.*, *Science* **324**, 1080 (2009).
12. J. A. Gorski *et al.*, *J. Neurosci.* **22**, 6309 (2002).
13. S. E. Ahmari, V. B. Risbrough, M. A. Geyer, H. B. Simpson, *Neuropsychopharmacology* **37**, 1216 (2012).
14. J. Mattis *et al.*, *Nat. Methods* **9**, 159 (2012).
15. L. M. Koran, G. L. Hanna, E. Hollander, G. Nestadt, H. B. Simpson; American Psychiatric Association, *Am. J. Psychiatry* **164** (suppl.), 5 (2007).
16. S. V. Shmelkov *et al.*, *Nat. Med.* **16**, 598, 1p, 602 (2010).
17. J. M. Welch *et al.*, *Nature* **448**, 894 (2007).
18. S. K. Chen *et al.*, *Cell* **141**, 775 (2010).
19. T. R. Insel, J. T. Winslow, *Psychiatr. Clin. North Am.* **15**, 813 (1992).
20. D. R. Rosenberg, M. S. Keshavan, *Biol. Psychiatry* **43**, 623 (1998).
21. L. R. Baxter Jr. *et al.*, *Am. J. Psychiatry* **145**, 1560 (1988).
22. K. Dzirasa *et al.*, *J. Neurosci.* **30**, 6387 (2010).
23. S. K. Bourne, C. A. Eckhardt, S. A. Sheth, E. N. Eskandar, *Front Integr Neurosci* **6**, 29 (2012).
24. A. M. Graybiel, S. L. Rauch, *Neuron* **28**, 343 (2000).
25. S. N. Haber, S. L. Rauch, *Neuropsychopharmacology* **35**, 1 (2010).
26. E. G. Antzoulatos, E. K. Miller, *Neuron* **71**, 243 (2011).
27. B. Abler, G. Grön, A. Hartmann, C. Metzger, M. Walter, *J. Neurosci.* **32**, 1329 (2012).
28. C. McCabe, Z. Mishor, P. J. Cowen, C. J. Harmer, *Biol. Psychiatry* **67**, 439 (2010).
29. D. Mataix-Cols *et al.*, *Arch. Gen. Psychiatry* **61**, 564 (2004).
30. J. F. Leckman *et al.*, *Depress. Anxiety* **27**, 507 (2010).
31. B. D. Greenberg *et al.*, *Mol. Psychiatry* **15**, 64 (2010).
32. P. P. de Koning, M. Figee, P. van den Munckhof, P. R. Schuurman, D. Denys, *Curr. Psychiatry Rep.* **13**, 274 (2011).

Acknowledgments: We thank H. B. Simpson and C. Kellendonk for critical discussions and reading of the manuscript and D. Flicker and M. Cloidt for behavioral scoring assistance. S.E.A. is supported by National Institute of Mental Health (NIMH) K08MH087718; the Louis V. Gerstner, Jr., Scholars Program; the Irving Institute for Clinical and Translational Research; the Gray Matters Foundation; the Leon Levy Foundation; and a Brain and Behavior Research Foundation NARSAD Young Investigator Award. M.A.K. is supported by

NIMH K01MH099371, the Sackler Institute, and a NARSAD Young Investigator Award. K.D. is supported by the Howard Hughes Medical Institute, NIH, California Institute for Regenerative Medicine, and the Defense Advance Research Projects Agency The Reorganization and Plasticity to Accelerate Injury Recovery (REPAIR) Program. J.G. is supported by NIH R01 MH096274, the Hope for Depression Research Foundation, and the International Mental Health Research Organization. R.H. is supported by the Hope for Depression Research Foundation.

Supplementary Materials
www.sciencemag.org/cgi/content/full/340/6137/1234/DC1
Materials and Methods
Figs. S1 to S5
Table S1
References (*33*–*43*)

3 January 2013; accepted 3 April 2013
10.1126/science.1234733

Geniculocortical Input Drives Genetic Distinctions Between Primary and Higher-Order Visual Areas

Shen-Ju Chou,[1]*† Zoila Babot,[1]* Axel Leingärtner,[1]‡ Michele Studer,[2]§ Yasushi Nakagawa,[1]|| Dennis D. M. O'Leary[1]¶

Studies of area patterning of the neocortex have focused on primary areas, concluding that the primary visual area, V1, is specified by transcription factors (TFs) expressed by progenitors. Mechanisms that determine higher-order visual areas (V^{HO}) and distinguish them from V1 are unknown. We demonstrated a requirement for thalamocortical axon (TCA) input by genetically deleting geniculocortical TCAs and showed that they drive differentiation of patterned gene expression that distinguishes V1 and V^{HO}. Our findings suggest a multistage process for area patterning: TFs expressed by progenitors specify an occipital visual cortical field that differentiates into V1 and V^{HO}; this latter phase requires geniculocortical TCA input to the nascent V1 that determines genetic distinctions between V1 and V^{HO} for all layers and ultimately determines their area-specific functional properties.

The neocortex is patterned into functionally distinct fields that include primary sensory areas, which receive modality-specific sensory input from thalamocortical axons (TCAs) that originate from the principal sensory nuclei of the dorsal thalamus (dTh), and higher-order sensory areas that are connected with the primary areas through intracortical projections (*1*). Studies of mechanisms that pattern the neocortex into areas, known as arealization, have focused on primary areas and have led to the prevailing model that genetic mechanisms intrinsic to the neocortex are predominant in arealization (*2*). Transcription factors (TFs) expressed in neocortical progenitors determine the size and position of primary areas (*2*–*5*) and regulate guidance information that governs the area-specific targeting of TCAs (*6*). However, roles for TCAs in arealization remain vague (*7*–*10*), and important features of arealization, such as differential gene expression in the embryonic neocortex that relates to nascent areas, develop independently of TCA input (*9, 10*).

Higher-order areas outnumber primary areas by roughly 10-fold; for example, in mouse, nine higher-order visual areas (V^{HO}) are positioned around the primary visual area (V1) within the occipital neocortex (*11*). However, mechanisms that specify and regulate differentiation of the particular properties of higher-order areas and distinguish them from primary areas have yet to be explored (*11, 12*). To perform genetic manipulations of dTh neurons required for these studies, we created RORα-IRES-Cre mice ($ROR\alpha^{Cre}$; fig. S1, A and B) with RORα function intact and expression of Cre recombinase driven by *RORα* regulatory elements (*13*). Crossing this $ROR\alpha^{Cre}$ mouse to conditional reporter lines (fig. S1) revealed Cre-mediated recombination in neurons of the principal sensory nuclei in dTh at embryonic day 14.5 (E14.5), shortly after they become postmitotic (*14*), with robust recombination in the dorsal lateral geniculate nucleus (dLG) (fig. S1, C to K), which forms the geniculocortical TCA projection that relays visual information from the eyes selectively to V1. Little or no recombination was detected in the neocortex through the end of the first postnatal week, encompassing the differentiation of cortical areas and the time frame of our study (fig. S1, C to K).

We crossed $ROR\alpha^{Cre}$ mice to mice in which the third exon of the COUP-TF1 gene is flanked by loxP sites, i.e. floxed (fl) COUP-TF1 [COUP-$TF1^{fl/fl}$ is described in (*5*)], because COUP-TF1 is strongly expressed in dLG, COUP-TF1 deletion diminishes axon growth (*15*), and most TCAs fail to reach the cortex in COUP-TF1–null mice (*16*). COUP-TF1–null mice are not useful for our studies because of viability issues and defects in cortical development (*16*). In contrast, the conditional knockout (cKO) mice ($ROR\alpha^{Cre/+}$ or $ROR\alpha^{Cre/Cre}$; $TF1^{fl/fl}$) were viable and retained robust COUP-TF1 expression in the neocortex (fig. S2, A and B), but COUP-TF1 was deleted from dLG by E15.5 (fig. S2, A and B), and dLG size in cKO mice progressively decreased from the wild-type (WT) size embryonically to virtually absent by postnatal day 7 (P7) (figs. S2, C and D, and S3).

To visualize TCA projections in the cortex, we first used serotonin [5-hydroxytryptamine (5-HT)] immunostaining on tangential sections of flattened P7 cortices. In P7 WT mice, 5-HT staining revealed the geniculocortical TCA projection from dLG to V1, as well as TCA projections from the ventroposterior nucleus (VP) to the primary somatosensory area (S1) and from the medial geniculate nucleus (MG) to the primary auditory area (A1) (Fig. 1A). In P7 cKO mice, 5-HT staining showed that TCA projections to S1 and A1 were intact, but the geniculocortical TCA projection to V1 was absent (Fig. 1A). The loss of geniculocortical input to V1 in P7 cKO mice was confirmed by anterograde and retrograde axon tracing from dLG and V1 (fig. S4, A and B) and by crossing the cKO mice to a ROSA26-GAP43-eGFP reporter line that labels TCAs by $ROR\alpha^{Cre}$ reporter activation (fig. S5A). Thus, conditional deletion of COUP-TF1 from dLG using the $ROR\alpha^{Cre}$ line resulted in deletion of the geniculocortical TCA projection by P7, but COUP-TF1 remained intact in the cortex.

To determine the time course of the geniculocortical TCA projection in cKO mice as compared to WT mice, we bred $ROR\alpha^{Cre}$ mice on either a WT ($TF1^{fl/+}$; $ROR\alpha^{Cre/+}$) or cKO ($TF1^{fl/fl}$; $ROR\alpha^{Cre/+}$ or $TF1^{fl/fl}$; $ROR\alpha^{Cre/Cre}$) background, to a conditional reporter line (Ai14 tdTomato) (*17*). Activation of the tdTomato reporter with the $ROR\alpha^{Cre}$ line labeled, at high resolution, geniculocortical TCAs from the dLG and TCAs from VP and MG projecting to S1 and A1 (Fig. 1B). Geniculocortical TCAs extend tangentially in the subplate and underlie the cortical plate (CP) of nascent V1 by E16.5, invade after birth the overlying V1 CP, and over the first postnatal week arborize in V1 layer 4, their predominant target layer (*18*). At E16.5, before TCAs invade the CP, the appearance of tdTomato-labeled TCAs was indistinguishable between WT and cKO mice, with

[1]Molecular Neurobiology Laboratory, The Salk Institute for Biological Studies, La Jolla, CA, USA. [2]Institute of Biology Valrose, INSERM, Nice, France.

*These authors contributed equally to this work.
†Present address: Institute of Cellular and Organismic Biology, Academia Sinica, Taipei, Taiwan.
‡Present address: University Cancer Center Hamburg, University Medical Center Hamburg-Eppendorf, Hamburg, Germany.
§Present address: Institute of Biology Valrose, iBV, UMR INSERM1091/CNRS7277/UNS, Nice, F-06108, France; and University of Nice Sophia-Antipolis, UFR Sciences, Nice, F-06108, France.
||Present address: Department of Neuroscience, Stem Cell Institute and Developmental Biology Center, University of Minnesota, Minneapolis, MN 55455, USA.
¶Corresponding author. E-mail: doleary@salk.edu